Probabilistic Engineering Mechanics 81 (2025) 103804

Contents lists available at ScienceDirect

Probabilistic Engineering Mechanics

journal homepage: www.elsevier.com/locate/probengmech

Influence of noise on First Passage Time maps and their use in damage detection

Kevin Theunissen [a,b,*], Vincent Denoël [a]

[a] Structural & Stochastic Dynamics, University of Liège, Belgium
[b] F.R.S.-FNRS, National Fund for Scientific Research, Belgium

ARTICLE INFO

Keywords:
Structural health monitoring
Sensitivity
Signal processing

ABSTRACT

Due to the aging of existing infrastructures and the growing of urbanisation among other things, Structural Health Monitoring has become a key element in various engineering fields. Numerous methods already exist to detect and localise damage to structures. However, the performances of such methods are reduced when subjected to unknown disturbances. In this paper, the influence of noise on a recent method based on the First Passage Time is studied. First, the description of the methodology is summarised and illustrated. Then, the efficacy of the method is assessed through four different scenarios. The first scenario considers the repeatability in identifying damage in ideal conditions, without any added noise. The other scenarios focus on the influence of additive loading (wind load) and measurement noise in detecting damage. It has been shown that the method excels in damage detection in each scenario. Indeed, even when the frequency change is approximately 1%, the method is still capable of identifying a small damage. However, in particular cases where the added measurement noise becomes too large, the method fails to distinguish the reference and damaged cases. Finally, due to the effectiveness of the bandpass filter in the processing of the method, the influence of wind load is limited, making the method efficient in detecting damage.

1. Introduction

Structural Health Monitoring (SHM) refers to the process of implementing a damage identification strategy for aerospace, civil, and mechanical engineering infrastructures [1]. It represents an approach in ensuring the safety, reliability, and longevity of infrastructures thanks to a wide variety of techniques, methodologies, and technologies that aim at monitoring the condition in structures to detect, assess, and mitigate potential damages [2]. With the increase of the global population, urbanisation grows [3] and existing infrastructures age [4]. SHM has gained in popularity with its applications spanning across civil infrastructures such as bridges [5,6], buildings [7], dams [8], pipelines [9], offshore structures [10,11], and more.

The objective of SHM lies in its proactive approach to maintenance and risk management. By implementing SHM systems, stakeholders can transition from reactive responses to structural failures to a proactive stance, wherein potential issues are identified and addressed before they escalate into catastrophic events [12]. This goal allows greater safety and reliability of infrastructures but also leads to significant cost savings [13] by optimising maintenance schedules, extending the service life of structures, and minimising downtime associated with repairs [14,15].

In addition, SHM involves the deployment of sensors and measurement devices to collect data regarding the structural response to environmental stresses and potential anomalies. This data is then analysed using various techniques that require the comparison of two states of the structure: the *healthy* or *reference* state and the *current* state that can become a *damaged* state if damage is detected [16]. To compare two states of the same structure, different techniques can be used, relying on, for example, the wave velocity inside the material [17], the modal curvature [18], the inverse of the structural stiffness matrix [19] or some modal parameters [20,21], such as eigenfrequencies, eigenmodes, and damping ratios. Finally, based on data analysis, stakeholders can make decisions concerning the maintenance and repair of the structure if damage is detected.

Another more recent technique is based on First Passage Times [22]. The efficiency of the methodology has already been assessed in [23] for damage detection and localisation. This new methodology appears as a good candidate for detecting small variations in a system. However, the influence of noise on the detection performances has not been thoroughly studied yet, a central question is assessing a damage identification procedure since this can make it less performant when

* Corresponding author at: Structural & Stochastic Dynamics, University of Liège, Belgium.
E-mail address: kevin.theunissen.pro@gmail.com (K. Theunissen).

https://doi.org/10.1016/j.probengmech.2025.103804
Received 3 September 2024; Received in revised form 16 May 2025; Accepted 1 July 2025
Available online 27 July 2025

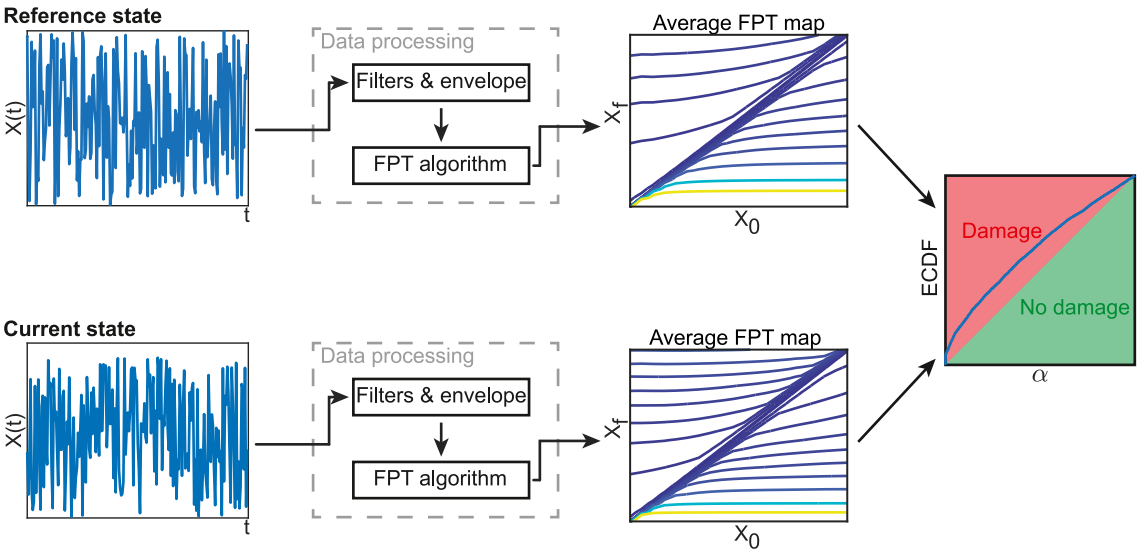

Fig. 1. Illustration of the chosen methodology for damage detection.

subjected to unknown disturbances. Therefore, in this article, the performances of the methodology are evaluated when the measured signal is corrupted by additive noise and an external loading to take into account the impact of these effects on the quality of damage detection.

Section 2 is dedicated to the summary of the methodology while Section 3 focuses on the influence of noise on the quality of the damage detection process. The performances of damage detection are assessed first in ideal conditions before studying the effect of an added unknown external loading and of additive noise to the measured signal.

2. Description of the chosen damage detection method

The damage detection method studied in this article is based on First Passage Time maps. In SHM, the comparison of these maps in the reference and current states is required for damage detection. In short, the method consists in measuring the response of the system to a given wideband loading, then processing measured accelerations (or other structural responses) to obtain their FPT maps. The comparison of such maps in the two states allows decisions about the presence of damage. While the methodology is comprehensively established in [23], in this section, the major steps are described.

2.1. First passage time maps

The First Passage Time (FPT) of a given signal is defined as the time required to reach a level X_f for the first time, starting from a level X_0. For a random signal, the FPT is a random variable. Indeed, for a given sampled signal, many samples of FPTs, corresponding to the multiple crossings, are computed and stored. Furthermore, various combinations (X_0, X_f) can be taken into account, which leads to a matrix that is also called a *map* [24]. Each cell of this map contains a collection of samples of FPTs, for a particular combination (X_0, X_f) which can be processed to assign, to each map cell, histograms or cumulated histograms, or more simply statistical moments. In the latter case, the map can also be referred to as the average of FPT map or the standard deviation of FPT map [25,26].

Computing these samples of FPTs is a time consuming task if no specific care is paid to the algorithmic approach. Therefore, they are not considered as a standard signal processing tool. However, an efficient algorithm [27] was developed to compute these samples of FPTs, making the computation of FPTs from any given signal feasible under trivially short computation time. Hence, this new tool has opened new perspectives for using FPTs as a signal processing technique in various fields of engineering, including SHM.

2.2. Damage detection based on these maps

The method based on FPT relies on different steps: data measurement, data processing, and the new algorithm [27], which efficiently computes First Passage Times from any time signal.

The first task consists in measuring the vibrations of the studied structure under a known loading, a band limited white noise whose Power Spectral Density (PSD) is constant in the frequency range $[f_{\min}; f_{\max}] = [0.9f, 1.1f]$ spanning a chosen natural frequency f. Due to environmental effects and the occurrence of damage, the natural frequencies of a structure may change over time. The proposed methodology currently works with one isolated natural frequency. The chosen frequency range is selected to ensure that this natural frequency is always located within the frequency range. If two natural frequencies are located in this frequency range, it is required to select another natural frequency or to manage sensors location to remove one of the two natural frequencies from the measurements before using the methodology to perform damage detection. There is also some freedom on the position of the loading point. In its current version, the methodology is based on a single mode observation, since the identification procedure requires a Hilbert transform, which is optimum for single mode responses. The acceleration (or any structural response) is measured by sensors placed at specific locations on the structure. Currently, the methodology only works with one sensor, but extensions could include multiple sensors.

The second task is dedicated to the processing of the measured data, which is divided into three distinct steps. First of all, a Butterworth bandpass filter of order 4 is applied to the measured data in the same frequency range $[f_{\min}; f_{\max}]$ [28]. This filter removes the undesired response in natural modes outside of the chosen frequency range. Even when the filter is applied only once, and a phase shift is introduced, the results computed by the FPT algorithm remain mainly unaffected.

The second filter acts like a linear filter and does not modify the phase of the signal. This filter aims to compensate for the slight possible discrepancy between the actual and target loadings. Indeed in an open-loop testing, it is possible that the PSD of the loading slightly differs from one test to another. To compensate for this undesired effect, a frequency content adjustment is performed.

Assuming that the system is linear time-invariant for each state and remains in a linear regime under the chosen loading, the following equations, in frequency domain, are obtained

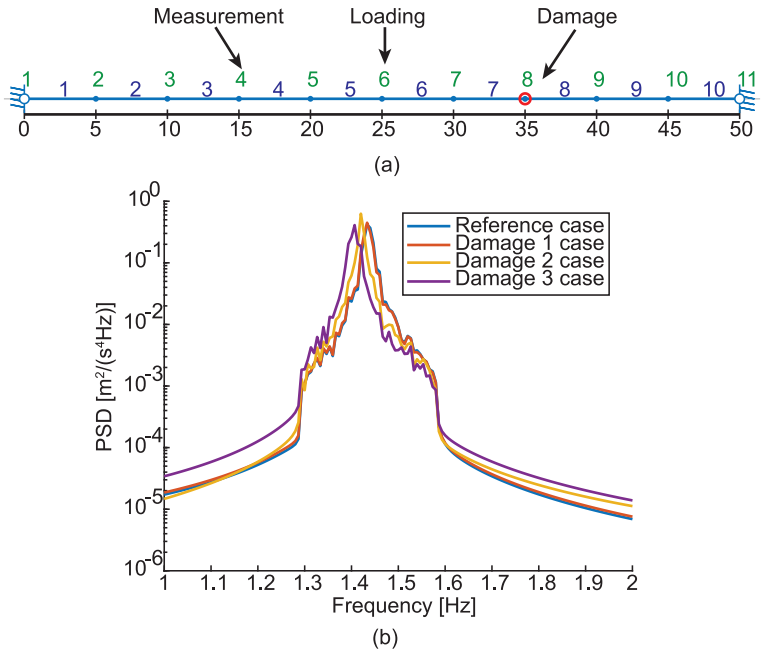

Fig. 2. (a) Numerical model and (b) PSDs of the first bending mode for the reference case and each damaged case.

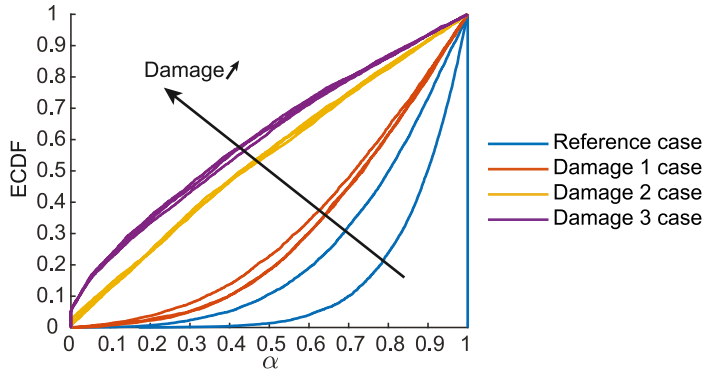

Fig. 3. Sensitivity of the chosen methodology - damage detection in ideal conditions.

$$HX_{ref} = F_{ref} \quad ; HX_{curr} = F_{curr} \tag{1}$$

where H is the transfer function in the current state, X is the measured structural response and F is the external loading, and indices *ref* and *curr* correspond to the healthy and current states.

Hence, the structural response $\widetilde{X}_{\text{ref}}$ that would have been measured in the current state if the forcing had been F_{ref} instead of the (slightly different) forcing F_{curr} is given by

$$\widetilde{X}_{ref} = \frac{F_{ref}}{F_{curr}} X_{curr}. \tag{2}$$

Then, the upper envelope is computed by applying the Hilbert transform. Many other fields also use the Hilbert transform for signal processing [29] and for detecting low damage level [30]. Moreover, by using the upper envelope, the fast dynamics of the measured data is removed, which could jeopardise the damage detection if a small shift in the natural period of the studied structure occurred.

Last but not least, the FPT map of this envelope is computed with the efficient FPT algorithm. As structural health monitoring requires the comparison of features, in the reference state and in the current state of the structure, to detect a damage if the difference is significant, FPT maps from these two different states are compared as shown in Fig. 1. The comparison of such maps relies on statistical hypothesis testing. Beforehand, the envelope signal is split into N signals of equal length. Hence, N FPT maps are obtained. Each cell of an FPT map contains a collection of FPTs. From this collection, an Empirical Cumulative Density Function (ECDF) is computed. For different given percentiles, the sample distribution of FPT histograms is compared in the reference and current states. From this test, for each chosen percentile, an α-value is obtained, quantifying in the sense of hypothesis testing the similarity between the sampled percentiles in the two states. Then, for a given combination (X_0, X_f), the average of the α-values is computed. If the average of α-values is close to 1, the ECDFs in the reference and current states are similar. If the average of α-values is close to 0, it is the opposite. These tests are repeated for each combination (X_0, X_f) inside the FPT map. At the end of this process, a new map, containing only the averages of α-values, is obtained, see [23] for more details about the method. To provide a visual representation of the damage detection, the ECDFs of α-values over the entire map are computed. If the reference and current states are similar, therefore, α-values are on average close to 1. This results in ECDFs of α-values that are close to the lower right corner. In addition, a simple rule, called the "rule-of-the-diagonal", has been proposed. If the ECDF of α-values is under the main diagonal, the current state is said to be undamaged. However, if the ECDF of α-values is above this diagonal, damage is detected and the current state is identified as a *damaged* state.

Table 1
Stiffness of the rotational spring, eigenfrequencies of the first bending mode in each case and their relative change with the healthy state.

	Rotational spring stiffness [Nm/rad]	First bending mode frequency [Hz]	Relative change [%]
Healthy case	∞	1.4360	0
Damaged case 1	10^{11}	1.4344	0.11
Damaged case 2	10^{10}	1.4205	1.08
Damaged case 3	$5 \cdot 10^{9}$	1.4055	2.12

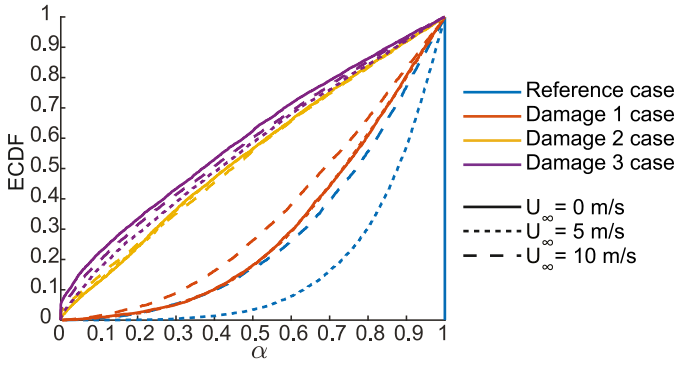

Fig. 4. Sensitivity of the chosen methodology - damage detection under wind load.

3. Influence of noise on first passage time maps

The methodology based on First Passage Times has shown great performances in ideal conditions [22,23]. However, the influence of external factors, such as wind load and measurement noise, can affect the capabilities of damage detection, especially if the loading changes as a result of inaccurate operating conditions, or if the signal is corrupted by noise. Therefore, this paper analyses the influence of such perturbations on the methodology.

3.1. Description of a numerical model

A numerical model has been created and virtually damaged to quantify the sensitivity of the methodology summarised in Section 2 concerning undesired perturbations. The numerical model is shown in Fig. 2(a). It models a 50-m bridge with 10 beam finite elements whose mass and stiffness matrices are given in Appendix. The size of the cross section has been chosen to represent a common bridge deck, whose width is 18 m. The material chosen for this bridge section is steel, whose Young Modulus E = 205000 MPa and density is equal to 7850 kg/m^3. The second moment inertia of the section is equal to 0.04 m^4 and its cross sectional area is equal to 0.2 m^2.

The input force, applied to the structure, is a band limited white noise with frequency band $[0.9f, 1.1f]$, where f is the chosen eigenfrequency, and is located at midspan (node 6). The response signal is the acceleration of the structure and is measured at node 4. This signal is obtained by using the Newmark scheme with a sampling frequency of 50 Hz. The damage is detected based on this sole acceleration. To simulate a damage in the numerical model, a rotational spring has been added at node 8. Alternative scenarios with other measurement loadings and damage points are discussed in Section 3.6.

To assess the sensitivity of the methodology, three different damaged cases are considered. The rotational spring stiffness is decreased from very large (10^{15} [Nm/rad]) in the healthy state, meaning that the connection between the seventh and eighth elements is perfectly rigid, to $5 \cdot 10^{9}$ [Nm/rad] in the third damaged case. By adding this rotational spring to the numerical model, it results in a decrease of the eigenfrequencies as shown in Fig. 2(b). A classical approach to damage detection would analyse this frequency change. Instead, the method proposed here is based on the FPT maps, as detailed earlier. The first bending mode has been chosen for the damage detection. The eigenfrequencies of the first bending mode in each case can be found in Table 1 as well as the relative change and the rotational spring stiffness.

Moreover, the simulation time has been fixed to 4 h. This duration is set long enough to obtain reproducible results for the statistical test.

Based on four different scenarios, the sensitivity of the proposed methodology is assessed. In the first scenario, the damage detection sensitivity is determined without any added perturbation, which represents the corner stage of the suggested methodology. Then, three other scenarios include wind loading as an unmeasured force, which is added to the external loading, an additive measurement noise that can directly pollute the measured signal, and the combination of the wind loading and the additive measurement noise. These four scenarios are studied in the rest of this section.

3.2. Scenario 1: Performances in ideal conditions

To study the sensitivity of the proposed methodology under damage only, in the absence of external disturbances, the damage detection is assessed considering three different samples of the input force for the reference case and each damaged case.

The ECDFs of α-values over the entire map are shown in Fig. 3 for the different configurations, while comparing them to the first loading, in the reference case. The remaining two reference cases are used to evaluate the sensitivity of the methodology to differentiate between very small damage, in damaged case 1, and variations resulting from test repeatability.

It can be observed that each damaged case gives distinct results from the others, resulting in a proper damage identification or at least a ranking of the various damage levels. The ECDFs are moving from the bottom right corner to the upper left corner in Fig. 3 when going from the reference case to the damaged cases. In the damaged case 1, the ECDFs are close to those of the reference case. Indeed, the modal parameters of the numerical model in the damaged case 1 do not differ significantly from those in the reference case. Indeed, the relative change in eigenfrequencies for the first bending mode is 0.1%

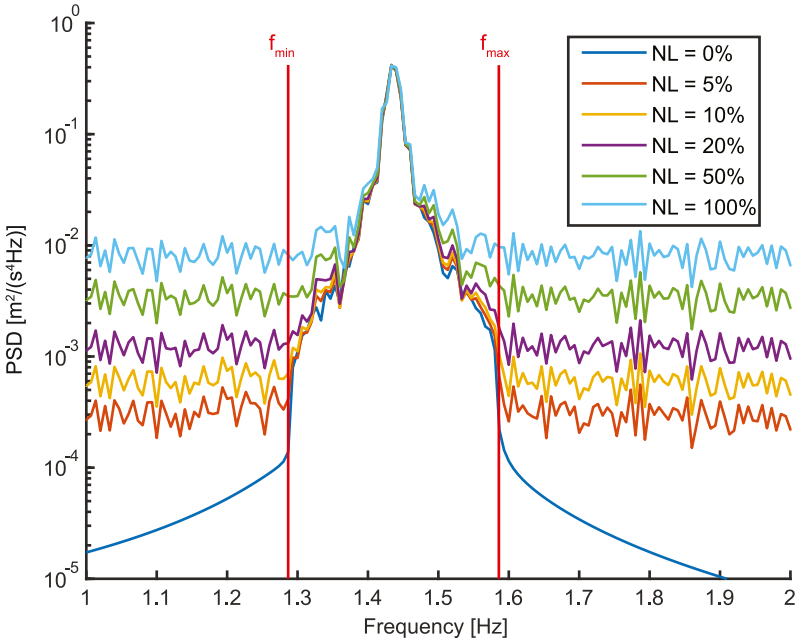

Fig. 5. PSDs of the measured acceleration of the structure under the input force and added noise. NL = Noise Level.

only. Then, the ECDFs are moving further away from the reference case in the damaged case 2 and even further in the damaged case 3, showing that the damage applied to the structure increases. Moreover, for each damaged case, the ECDFs of α-values are more or less superimposed, meaning that the method is repeatable in identifying the damaged cases.

3.3. Scenario 2: Influence of additive unmeasured loading

To further assess the sensitivity of the performances of the methodology, unmeasured wind loads are applied to the structure in addition to the input force. These wind loads are distributed along the entire bridge deck. The resulting wind forces are integrated over each element and subsequently transformed into nodal forces. At each node of the model, the applied force is given by

$$F_{i,\text{wind}}(t) = \frac{1}{2}\rho C_L B \left(U_\infty + u_i(t)\right)^2 L_{\text{elem}} \tag{3}$$

where $\rho = 1.22$ kg/m^3 is the air density, $B = 18$ m is the width of the bridge deck, U_∞ is the average wind speed, $u_i(t)$ is the u component of the turbulent wind, $L_{\text{elem}} = 5$ m is the length of one element, and C_L is the lift coefficient, which is equal to 0.9 [31]. In this example, two different average wind speeds have been chosen: $U_\infty = 5$ and $U_\infty = 10$ m/s. The case $U_\infty = 0$ m/s corresponds to the case without added wind, identical to the one treated in the previous subsection. The u component is described by the PSD of Von Karman, given by

$$S_u(f) = \frac{L \cdot \sigma_u^2}{\pi U_\infty \left(1 + 70.7\left(f \cdot \frac{L}{U_\infty}\right)^2\right)^{5/6}} \tag{4}$$

where $L = 30$ m is the turbulence length scale and σ_u is the standard deviation of the turbulent wind and is equal to 1 and 2 m/s when U_∞ is equal to 5 and 10 m/s respectively.

Moreover, the wind loads are spatially correlated. The coherence PSD is the following [32]

$$\Gamma_u(\omega) = e^{-\frac{C\cdot\omega\cdot\Delta x}{4\pi U_\infty}} \tag{5}$$

where $C = 11.5$ is the coefficient of coherence and Δx is the distance between two nodes.

Synthetic wind turbulence samples, based on the PSD and coherence functions, are generated using standard methods [33]. From these time series, the individual wind components $u_i(t)$ are derived and subsequently used in Eq. (3) to compute the nodal forces. In this study, a sample duration of four hours with a sampling frequency of 50 Hz has been used.

Again, the FPT maps of the acceleration are established and compared with the method described in Section 2. All variants (three wind speeds and four reference/damaged cases) are compared to the reference case without damage and wind. The ECDFs of the α-values obtained in all those variants are shown in Fig. 4.

- A clear distinction can be made for each case, meaning that the damage detection is only slightly disturbed by these wind loads and is feasible.
- For each wind speed, each damaged case is well separated from the others.
- When the wind speed is approaching 10 m/s, the reference case is close to the damaged case 1 without or with the smallest wind load (5 m/s).
- The influence of the wind on the methodology is limited due to the bandpass filter used in the processing step. Indeed, the PSD of the wind is relatively flat and low in the chosen frequency range $[f_{\min}, f_{\max}]$ so that the amount of energy in that higher frequency band is rather limited.

3.4. Scenario 3: Influence of additive measurement noise

The next scenario takes into account the noise that affects the measured signal. This noise is generated as a band-limited white noise in the range [0.5;5]Hz. Different Noise Levels (NL) have been selected, going from 5% to 100%. The NL is defined as

$$\text{NL} = \frac{\sigma_{\text{signal+noise}} - \sigma_{\text{signal}}}{\sigma_{\text{signal}}} = \sqrt{1 + (\text{N/S})^2} - 1 \tag{6}$$

where σ is the standard deviation and N/S is the noise over signal ratio.

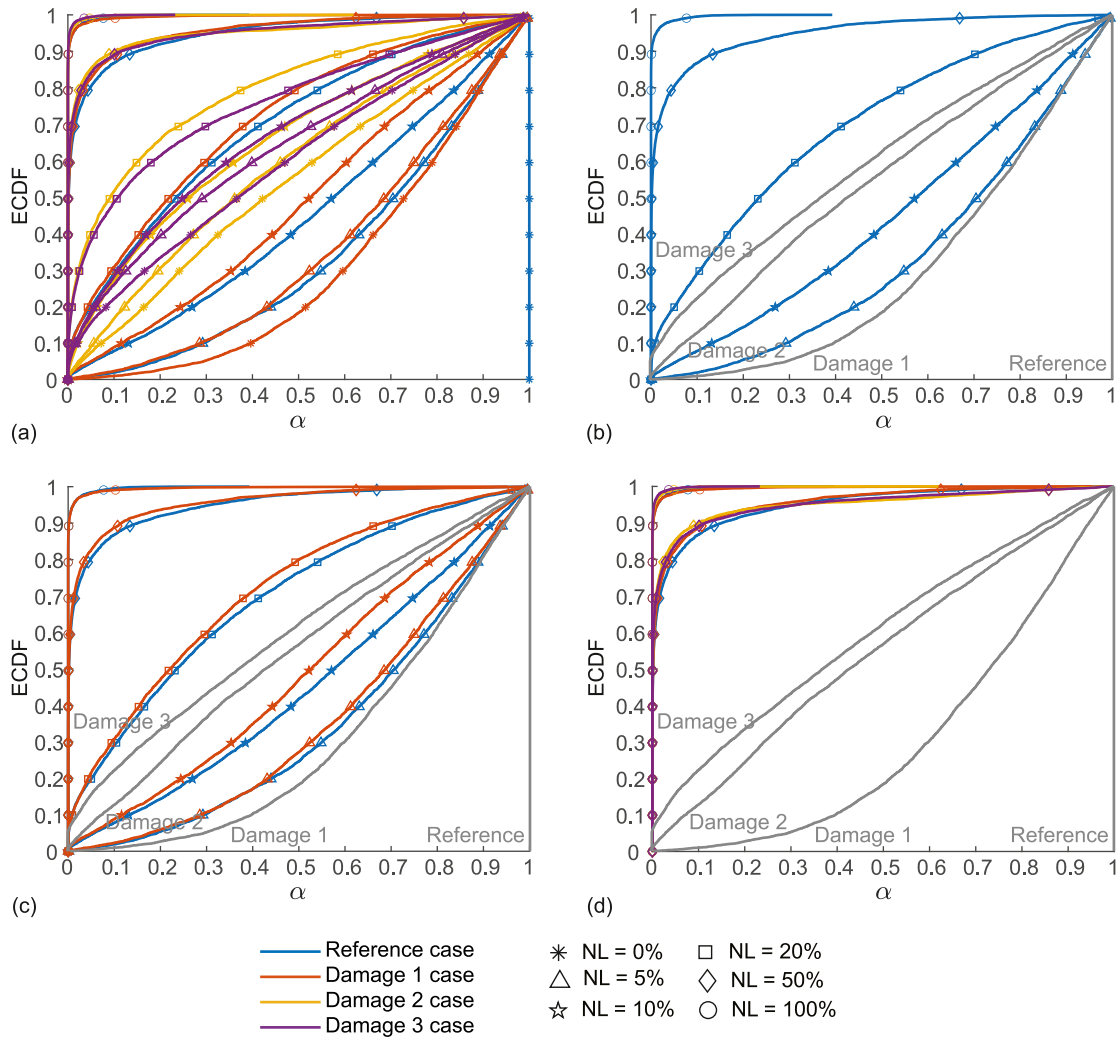

Fig. 6. Sensitivity of the chosen methodology - damage detection under different noise levels: (a) influence of the noise in each state, (b) influence of the noise in the reference case, (c) influence of the noise in the reference case and damaged case 1, and (d) influence of the noise at noise levels 50% and 100%. NL = Noise Level.

When NL = 100%, the standard deviation of the noisy signal is twice greater than the reference signal without noise. The effect of the added noise can be directly seen in the PSDs shown in Fig. 5. By increasing the noise level, the frequency ranges that are mainly subjected to changes are those close to $f_{\min} = 1.29$ Hz and $f_{\max} = 1.58$ Hz. Thanks to the bandpass filter, modifications outside the frequency range $[f_{\min}; f_{\max}]$ is discarded. Hence, after filtering, the net noise level is, in fact, equal to 1.2% and 8.7% compared to 20% and 100% respectively without filtering.

Nevertheless, in Fig. 6, it can be seen that the noise greatly affects damage detection. Except for Fig. 6(a), the ECDFs of the signal without noise are shown in grey to improve the comparison with ECDFs of the signals with noise. In Fig. 6(b), it can be seen that a noise level of 5% for the reference already exceeds the threshold of the damaged case 1 without noise. This is expected since the two cases are similar to each other. However, a noise level of 20% for the reference case is required to surpass the threshold imposed by the damaged cases 2 and 3. In Fig. 6(c), it can be observed that for the same noise level, the ECDFs of the α-values in the reference case are always slightly lower than the ECDFs of the α-values in the damaged case 1. This shows that the damage detection is still performing well for the same noise level and is able to make distinction between two systems with close modal properties. In Fig. 6(d), it can be seen that when the noise level is important, superior or equal to 50%, the ECDFs of the α-values for each case almost coincide. In this case, the damage detection fails and is not able to make the distinction between a small damage, as in damaged case 1, and a higher damage, like in damaged cases 2 and 3.

3.5. Scenario 4: Influence of both additive loading and measurement noise

The last scenario consists in considering the effect of the additive loading and the measurement noise at the same time. The influence of this combination is shown in Fig. 7(a) for each case. This figure is challenging to interpret and has been split into 3 separate figures for better readability. In Fig. 7(b), it can be observed that when the wind speed is equal to 10 m/s, for each noise level, the efficiency of the methodology is reduced. On the other hand, when the wind speed is equal to 5 m/s, the ECDFs of α-values are close to the ECDFs when there is no wind loading, resulting in a slight variation compared to the impact of the measurement noise. In Fig. 7(c), the influence of the wind loading, when the wind speed is equal to 10 m/s, makes the methodology unable to distinguish between the reference case and the damaged case 1. Indeed, the ECDFs of α-values are closer to the upper left corner in the reference for a wind speed equal to 10 m/s than for the ECDFs in the damaged case 1 for wind speeds equal to 0 and 5 m/s. This observation is particularly noticeable when the noise level is equal to 5% and 10%. Finally, in Fig. 7(d), the influence of the wind loading is not significant as all ECDFs of α-values are more or less superimposed when the noise level is equal to 50% and 100% respectively. In this case, the methodology is unfortunately unable to differentiate the reference case from any damaged case.

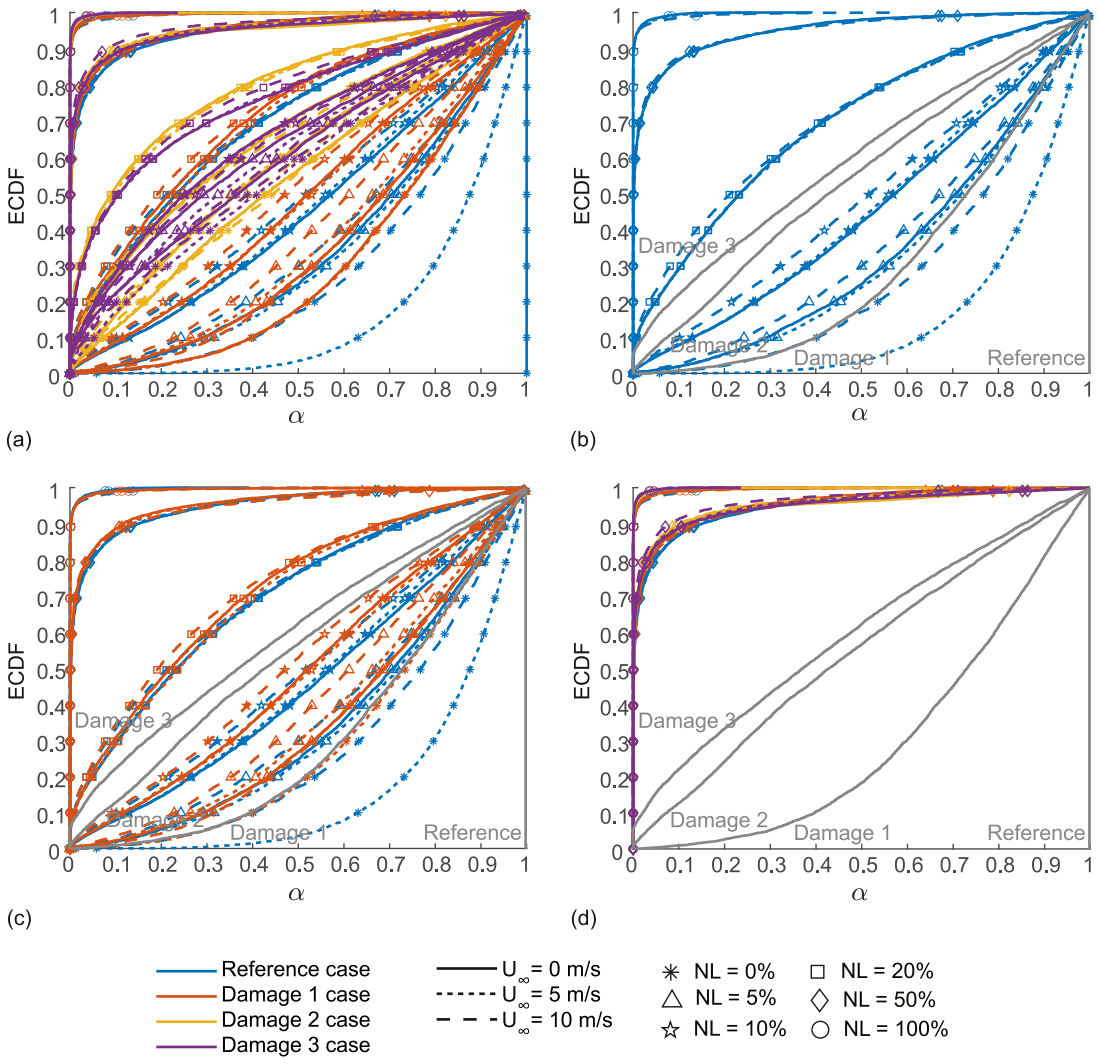

Fig. 7. Sensitivity of the chosen methodology - damage detection under different noise levels and wind speeds: (a) influence of the noise and wind loading in each state, (b) influence of the noise and wind loading in the reference case, (c) influence of the noise and wind loading in the reference case and damaged case 1, and (d) influence of the noise and wind loading at noise levels 50% and 100%. NL = Noise Level.

3.6. Alternative scenarios

This subsection discusses the potential influence of measurement points, loading points, and damage locations on the conclusions drawn in this article.

When the measurement point is changed, the measured accelerations remain qualitatively similar. Indeed, as the PSD of the loading remains centred around the first bending mode, the resulting accelerations differ only in amplitude. Given that the same signal-to-noise ratios as those used throughout the study are maintained, the conclusions remain unchanged.

A similar observation applies to the loading location. When the excitation force is applied to a different node, the energy injected into the system is altered due to the localised nature of the input. Since the frequency content of the loading PSD contains only the first bending mode, only the amplitude of the measured accelerations is impacted. Consequently, when the same signal-to-noise ratios are considered, the derived conclusions are not affected.

Regarding the damage location, moving the damage to a different node can be compensated by appropriately adjusting the local stiffness reduction to produce the same frequency shift observed in the original configuration. Since the analysis focuses on the first bending mode, the damage can be placed at any internal node of the numerical model without compromising the validity of the conclusions.

In summary, the choice of measurement, loading, and damage points does not affect the generality of the conclusions. Therefore, the current setup sufficiently captures the phenomena under investigation.

4. Conclusion

A damage detection methodology based on FPT [22,23] has been considered in this paper. While its performances have already been assessed previously, the novelty of this article is to evaluate the performances of the same methodology when the measured signal is corrupted by an additional noise and an external loading. To do so, the sensitivity of a damage detection methodology based on FPT has been assessed through four different scenarios. Globally, it has been shown that the methodology performed well in damage detection in each scenario. Indeed, the methodology is capable of detecting small damage even when the frequency change is approximately 1% or below.

However, the effects of the additive loading and the measurement noise reduce the performances of the methodology, especially to distinguish very small damage. For a noise level below 20%, the damaged cases 2 and 3 are still identified as such, which corresponds to a frequency change of 1 and 2%. Moreover, for large added measurement noise (noise level of 50% and 100%), the methodology fails to detect damage as it is impossible to make a distinction between the reference

case and any damaged case. In particular situations where measurement noise is large, an improvement in the measurement acquisition method is required to reduce the noise level.

Finally, the influence of the wind load is minimal on the methodology due to the effectiveness of the bandpass filter. The PSD of the wind load exhibits a relatively flat and low profile within the frequency range around the natural frequency. Additionally, the bandpass filter discards frequencies below the selected threshold $f_{\min}$, further reducing the influence of wind load.

The methodology has already been successfully tested in laboratory conditions on two different structures: a steel strip and a 25-meter prestressed concrete beam [22]. The promising results obtained in both cases demonstrate the potential of the methodology for real-world applications. For practical implementation on various structures, a shaker, with appropriate mass and dimension, can be employed to accommodate the specific dynamic characteristics of the target structure.

For future work, artificial intelligence could be combined with this method to improve the results based on pattern recognition. Indeed, the influence of the additive loading and the measurement noise could possess a specific signature on the FPT maps. By recognising these patterns, it could be possible to discard the impact of the additive loading and the measurement noise as well as other external parameters. This approach has not been included in this paper since two configurations were compared by the distribution of the α-values throughout the entire map, an operation that discards the specific arrangement of the α-values in the map.

CRediT authorship contribution statement

Kevin Theunissen: Methodology, Software, Visualization, Conceptualization, Writing – original draft, Investigation, Validation. **Vincent Denoël:** Supervision, Conceptualization, Validation, Funding acquisition, Writing – review & editing, Methodology, Project administration, Visualization, Investigation.

Declaration of competing interest

The authors declare that they have no known competing financial interests or personal relationships that could have appeared to influence the work reported in this paper.

Acknowledgement

K. Theunissen has been supported by the Belgian Fund for Scientific Research.

Appendix

Stiffness and mass matrices of the elements of the numerical model

In this Appendix, the stiffness, consistent-mass and consistent geometric-stiffness are written for a given element of length L [34]. Each beam element contains 2 nodes with two displacements allowed for each node: the transversal displacement v and the in-plane rotation θ. The parameters E and I are respectively the Young's modulus and the inertia of the element. The parameter $\bar{m}$ takes into account the uniformly distributed mass of the element.

Stiffness matrix

This matrix takes into account the stiffness of the elements at their nodes. For the special case of a uniform beam segment, the stiffness matrix can be expressed by

$$\begin{Bmatrix} f_{S1} \\ f_{S2} \\ f_{S3} \\ f_{S4} \end{Bmatrix} = \frac{2EI}{L^3} \begin{bmatrix} 6 & -6 & 3L & 3L \\ -6 & 6 & -3L & -3L \\ 3L & -3L & 2L^2 & L^2 \\ 3L & -3L & L^2 & 2L^2 \end{bmatrix} \begin{Bmatrix} v_1 \\ v_2 \\ \theta_1 \\ \theta_2 \end{Bmatrix}$$

Consistent-mass matrix

This matrix takes into account the mass distribution of the elements. In the special case of a beam with uniformly distributed mass the consistent-mass matrix can be written as

$$\begin{Bmatrix} f_{I1} \\ f_{I2} \\ f_{I3} \\ f_{I4} \end{Bmatrix} = \frac{\bar{m}L}{420} \begin{bmatrix} 156 & 54 & 22L & -13L \\ 54 & 156 & 13L & -22L \\ 22L & 13L & 4L^2 & -3L^2 \\ -13L & -22L & -3L^2 & 4L^2 \end{bmatrix} \begin{Bmatrix} \ddot{v}_1 \\ \ddot{v}_2 \\ \ddot{\theta}_1 \\ \ddot{\theta}_2 \end{Bmatrix}$$

Data availability

Data will be made available on request.

References

[1] Charles R. Farrar, Keith Worden, An introduction to structural health monitoring, Philos. Trans. R. Soc. A: Math. Phys. Eng. Sci. 365 (1851) (2007) 303–315.
[2] Keith Worden, Janice M. Dulieu-Barton, An overview of intelligent fault detection in systems and structures, Struct. Heal. Monit. 3 (1) (2004) 85–98.
[3] Gianluca Egidi, Luca Salvati, Sabato Vinci, The long way to tipperary: City size and worldwide urban population trends, 1950–2030, Sustain. Cities Soc. 60 (2020) 102148.
[4] Michael Carey Brown, Jose P. Gomez, Maureen L. Hammer, John M. Hooks, et al., Long-Term Bridge Performance High Priority Bridge Performance Issues, Technical Report, United States. Federal Highway Administration. Office of Infrastructure, 2014.
[5] Zhihang Deng, Minshui Huang, Neng Wan, Jianwei Zhang, The current development of structural health monitoring for bridges: A review, Buildings 13 (6) (2023) 1360.
[6] Francesco Lo Iacono, Giacomo Navarra, Maria Oliva, Structural monitoring of "Himera" viaduct by low-cost MEMS sensors: characterization and preliminary results, Meccanica 52 (2017) 3221–3236.
[7] Arvindan Sivasuriyan, Dhanasingh Sivalinga Vijayan, Wojciech Górski, Łukasz Wodzyński, Magdalena Daria Vaverková, Eugeniusz Koda, Practical implementation of structural health monitoring in multi-story buildings, Buildings 11 (6) (2021) 263.
[8] Arvindan Sivasuriyan, Dhanasingh Sivalinga Vijayan, Ravindiran Munusami, Parthiban Devarajan, Health assessment of dams under various environmental conditions using structural health monitoring techniques: a state-of-art review, Environ. Sci. Pollut. Res. (2021) 1–12.
[9] Mahjoub El Mountassir, Slah Yaacoubi, Fethi Dahmene, Reducing false alarms in guided waves structural health monitoring of pipelines: Review synthesis and debate, Int. J. Press. Vessels Pip. 188 (2020) 104210.
[10] Hadi Pezeshki, Hojjat Adeli, Dimitrios Pavlou, Sudath C. Siriwardane, State of the art in structural health monitoring of offshore and marine structures, in: Proceedings of the Institution of Civil Engineers-Maritime Engineering, vol. 176, (no. 2) Thomas Telford Ltd, 2023, pp. 89–108.
[11] Nandar Hlaing, Pablo G. Morato, Jannie S. Nielsen, Peyman Amirafshari, Athanasios Kolios, Philippe Rigo, Inspection and maintenance planning for offshore wind structural components: integrating fatigue failure criteria with Bayesian networks and Markov decision processes, Struct. Infrastruct. Eng. 18 (7) (2022) 983–1001.
[12] Andrea Orgnoni, Rui Pinho, Matteo Moratti, Nicola Scattarreggia, Gian Michele Calvi, et al., Critical review and modelling of the construction sequence and loading history of the collapsed Morandi Bridge, Int. J. Bridg. Eng 10 (3) (2022) 37–62.
[13] Vincenzo Cusati, Salvatore Corcione, Vittorio Memmolo, Impact of structural health monitoring on aircraft operating costs by multidisciplinary analysis, Sensors 21 (20) (2021) 6938.
[14] Jannie S. Nielsen, Dmitri Tcherniak, Martin D. Ulriksen, A case study on risk-based maintenance of wind turbine blades with structural health monitoring, Struct. Infrastruct. Eng. 17 (3) (2021) 302–318.
[15] Pablo G. Morato, Konstantinos G. Papakonstantinou, Charalampos P. Andriotis, Jannie Sønderkær Nielsen, Philippe Rigo, Optimal inspection and maintenance planning for deteriorating structural components through dynamic Bayesian networks and Markov decision processes, Struct. Saf. 94 (2022) 102140.
[16] Daniel J. Inman, C.R. Farrar, Vicente Lopes, Valder Steffen, Lopes, Steffen, Damage prognosis for aerospace, civil and mechanical systems preface, 2005, URL https://api.semanticscholar.org/CorpusID:106607472.
[17] Rahim Gorgin, Ying Luo, Zhanjun Wu, Environmental and operational conditions effects on Lamb wave based structural health monitoring systems: A review, Ultrasonics 105 (2020) 106114.
[18] Mahendran Govindasamy, Gopalakrishnan Kamalakannan, Chandrasekaran Kesavan, Ganesh Kumar Meenashisundaram, Damage detection in glass/epoxy laminated composite plates using modal curvature for structural health monitoring applications, J. Compos. Sci. 4 (4) (2020) 185.

[19] Sebastian Schommer, Viet Ha Nguyen, Stefan Maas, Arno Zürbes, Model updating for structural health monitoring using static and dynamic measurements, Procedia Eng. 199 (2017) 2146–2153.
[20] Scott W. Doebling, Charles R. Farrar, Michael B. Prime, Daniel W. Shevitz, Damage Identification and Health Monitoring of Structural and Mechanical Systems from Changes in Their Vibration Characteristics: A Literature Review, Los Alamos National Lab.(LANL), Los Alamos, NM (United States), 1996.
[21] Onur Avci, Osama Abdeljaber, Serkan Kiranyaz, Mohammed Hussein, Moncef Gabbouj, Daniel J. Inman, A review of vibration-based damage detection in civil structures: From traditional methods to machine learning and deep learning applications, Mech. Syst. Signal Process. 147 (2021) 107077.
[22] Kevin Theunissen, A Methodology based on First Passage Times for Structural Health Monitoring in Civil Engineering (Ph.D. thesis), ULiège - Université de Liège, 2024.
[23] Kevin Theunissen, Edouard Verstraelen, Vincent Denoël, Damage detection and localisation based on First Passage Time histograms, Structural Health Monitoring (2024) submitted for publication.
[24] Hélène Vanvinckenroye, Vincent Denoël, Average first-passage time of a quasi-Hamiltonian Mathieu oscillator with parametric and forcing excitations, J. Sound Vib. 406 (2017) 328–345.
[25] Hélène Vanvinckenroye, Thomas Andrianne, Vincent Denoël, First passage time as an analysis tool in experimental wind engineering, J. Wind Eng. Ind. Aerodyn. 177 (2018) 366–375.
[26] Hélène Vanvinckenroye, Vincent Denoël, Second-order moment of the first passage time of a quasi-Hamiltonian oscillator with stochastic parametric and forcing excitations, J. Sound Vib. 427 (2018) 178–187.
[27] Kevin Theunissen, Vincent Denoël, An efficient algorithm for the computation of the First Passage Time maps of a given signal, Mech. Syst. Signal Process. 207 (2024) 110884.
[28] Stephen Butterworth, et al., On the theory of filter amplifiers, Wirel. Eng. 7 (6) (1930) 536–541.
[29] Yi-Wen Liu, Hilbert transform and applications, in: S. Salih (Ed.), Fourier Transform Applications, InTech, Croatia, 2012, pp. 291–300.
[30] F. Lo Iacono, G. Navarra, A. Pirrotta, A damage identification procedure based on Hilbert transform: experimental validation, Struct. Control. Heal. Monit. 19 (1) (2012) 146–160.
[31] Eurocode EN 1991–1–4 Eurocode 1: Actions on structures - Part 1-4: General actions - Wind actions.
[32] Vincent Denoël, Application des méthodes d'analyse stochastique à l'étude des effets du vent sur les structures du génie civil (Ph.D. thesis), F.R.S.-FNRS - Fonds de la Recherche Scientifique [BE], ULiège - Université de Liège, 2005.
[33] Masanobu Shinozuka, George Deodatis, Simulation of stochastic processes by spectral representation, Appl. Mech. Rev. 44 (4) (1991) 191–204, http://dx.doi.org/10.1115/1.3119501, arXiv:https://asmedigitalcollection.asme.org/appliedmechanicsreviews/article-pdf/44/4/191/5435905/191_1.pdf.
[34] Clough Ray W., Penzien Joseph, Dynamics of Structures, Computer & Structures, 1995.